Emulating "Chaos + Chaos = Order" in Chen's Circuit of Fractional Order by Parameter Switching

WALLACE K.S. TANG
Department of Electronic Engineering,
City University of Hong Kong, Hong Kong
eekstang@cityu.edu.hk

MARIUS-F. DANCA*
Department of Mathematics and Computer Science,
Avram Iancu University of Cluj-Napoca, Romania
and
Romanian Institute of Science and Technology,
Cluj-Napoca, Romania
danca@rist.ro

Received (to be inserted by publisher)

In this paper, the effect of the parameter switching (PS) algorithm in a fractional order chaotic circuit is investigated both in simulation and experiment. The Chen system of fractional order is focused and realized in an electronic circuit. By designing a switching circuit, the PS algorithm is implemented and it is the first time, the paradoxical "chaos + chaos = order" is presented in an electronic circuit. Both the simulation and experimental results confirm that the obtained attractor under switching approximates the attractor of the time-averaged model. Some important design issues for the circuitry realization of the PS scheme are pointed out. Finally, our work confirms the practical usage of PS algorithm in potential applications such as attractor synthesis and chaos control.

Keywords: Chaos, Chen's circuit, fractional order system, parameter switching.

1. Introduction

Parameter Switching (PS) is a known topic in the study of the dynamics of a large class of continuous and discrete nonlinear systems. Its potential applications in attractors approximation, chaos control and anticontrol, have been explored [Danca *et al.*, 2008]. In [Mao *et al.*, 2010], it has been proven that under the PS algorithm, the dynamics of a class of continuous-time systems, modeled by integer-order differential equations, converges to its time-averaged model. The PS algorithm has also been successfully applied to other classes of systems such as continuous systems of fractional-order, discontinuous systems of integer and fractional order, and discrete-time system of real and complex variables [Danca *et al.*, 2014]. In addition, some new intriguing properties have been revealed in [Danca *et al.*, 2013] when applying the PS algorithm to fractals. However, all these previous work are only theoretical or based on numerical simulations. There

*corresponding author

is no suggestion for the physical implementation of PS algorithm, nor experimental study of the use of PS algorithm.

In order to justify the practicability of the PS algorithm, it is essential to demonstrate its effectiveness in practical system via experiments. This leads to the objectives of this paper, i.e. to demonstrate how the PS algorithm can be implemented and how to obtain any desired attractor of a given system in practice. For this purpose, a fractional-order chaotic system is considered. Complex systems with dynamic fractional behaviours can be found in physics, chemistry, rheology, etc, with examples including ultra-capacitor [Parreno *et al.*, 2010], beam heating process [Dzielinski *et al.*, 2010], large RC networks [Galvao *et al.*, 2013], and so on. To model and analyze this class of systems, fractional calculus serves as an essential tool. Recently, it also ignited the design of fractional order chaotic systems which have received a lot of attention from the field of nonlinear sciences. Examples include fractional order Chua system [Gammoudi & Feki, 2013; Liu *et al.*, 2009], Chen system [Asheghan *et al.*, 2011], Liu system [Hegazi *et al.*, 2013], van der Pol oscillator [Shen *et al.*, 2014], Lorenz system [Sun *et al.*, 2010], Pehlivan–Uyaroğlu spiking oscillator [Kingni *et al.*, 2015], multi-wing chaotic systems [Jia *et al.*, 2014; Xu, 2014; Zhang & Yu, 2011], just to name a few. In addition to system modeling, the synchronization and control of these fractional-order chaotic systems have also been investigated [Agrawal *et al.*, 2012; Hegazi *et al.*, 2013; Lin *et al.*, 2011; Wang *et al.*, 2009].

There are several definitions of fractional derivatives, including Grünwald-Letnikov fractional derivative, Reimann-Liouville fractional derivative and Caputo fractional derivative (see eg. [Caputo, 1967; Oldham & Spanier, 1974; Podlubny, 2002]). Since nonlinear fractional-order differential equations (FDEs) are generally unable to be solved analytically, numerical integration method such as the Adams-Basforth-Moulton predictor-corrector scheme (ABM) [Diethelm *et al.*, 2002] is used. Analysis has also been made in the frequency domain, which leads to the approximation of the fractional power frequency response. Frequency domain approximation is important, as it forms the basis for the circuit realization of fractional order systems [Jia *et al.*, 2014; Liu *et al.*, 2009]. It should be remarked that a fractional order system may act quite differently as compared with its counterpart in integer-order system. Moreover, different methods may result in different solutions, and hence they should be handled carefully [Kaslik & Sivasundaram, 2012; Tavazoei & Haeri, 2010; Yazdani & Salarieh, 2011].

In this paper, we designed a Chen circuit with fractional order, together with a circuit implementation of PS algorithm. By switching a system component in the designed circuit, it is verified that stable cycles can be obtained from two or more chaotic attractors. This approach is robust and multiple options are possible to obtain the same attractor.

The organization of this paper is as follows. In Sec. 2, the PS algorithm is revisited and the example of the fractional-order Chen system is considered. In Sec. 3, the fractional-order Chen circuit and the switching circuit are designed. By comparing the obtained attractors from simulation and experiments, the corresponding switching parameters in simulation and experiment are connected. The PS algorithm is then applied to the fractional-order Chen circuit to approximate stable cycles and the results are shown in Sec. 4. Discussions are also made to explain the important issues related to the realization. Finally, conclusions are given in Sec. 5.

2. Parameter Switching Algorithm

2.1. *IVP and PS Algorithm*

Let's consider the following general Initial Value problem (IVP) of fractional order

$$D_*^q x(t) = f(x(t)) + pAx(t), \quad x(0) = x_0, \quad t \in [0, T], \tag{1}$$

with $x_0 \in \mathbb{R}^n$, $T > 0$, $p \in \mathbb{R}$ the control parameter, $A \in L(\mathbb{R}^n)$ and $f : \mathbb{R}^n \to \mathbb{R}^n$ a nonlinear function. To avoid the use of fractional-order initial conditions, D_*^q stands for Caputo's derivative which is defined by

$$D_*^q x(t) = \frac{1}{\Gamma(\lceil q \rceil - q)} \int_0^t (t-\tau)^{\lceil q \rceil - q - 1} D^{\lceil q \rceil} x(\tau) d\tau, \tag{2}$$

where $0 < q \leq 1$ and $\Gamma(z) = \int_0^\infty t^{z-1}e^{-t}dt$ is the Gamma function with $z \in \mathbb{C}$ and $\Re(z) > 0$.

The IVP (1) models a large class of continuous nonlinear and autonomous dynamical systems of fractional order depending on a single real control parameter such as Chen system, Lorenz system, Rössler system, Hindmarsh-Rose system, Rabinovich-Fabrikant system, Lotka-Volterra system, some classes of minimal networks and many others.

To numerically solve the FDE (1), ABM predictor-corrector scheme with fixed step-size h is employed [Diethelm *et al.*, 2002]. Now, we consider the parameter p in (1) being switched periodically among a finite set of values, denoted by $\mathcal{P}_N = \{p_1, p_2, ..., p_N\}$ for $N > 1$, using the PS algorithm. The procedures are given as follows: For the first m_1 integration steps, $p = p_1$, then for the next m_2 steps, $p = p_2$ and so on till the m_N steps for which $p = p_N$. This cycle repeats with switching for a period of $(m_1 + m_2 + ... + m_N)h$, until the integration interval I ends. The variable m_i, is then considered as the "weight" of p_i, for $i = 1, 2, ..., N$.

The PS convergence shows that the resultant "switched" solution will approximate numerically the "averaged" solution, obtained by substituting the parameter p by the following time-average of the switched values, p^*:

$$p^* := \frac{\sum_{i=1}^N m_i p_i}{\sum_{i=1}^N m_i}. \tag{3}$$

In this paper, for a given initial condition, an *attractor* (chaotic attractor or stable cycle) represents the numerical approximation of the ω-limit set after neglecting a sufficiently long period of transients [Foias & Jolly, 1995].

In [Mao *et al.*, 2010], the following property is mathematically proved for integer order system ($q = 1$)[1].

Property 1. *[Mao et al., 2010]* Any attractor of the system can be numerically approximated by the PS algorithm with arbitrary accuracy.

Schematically, for a given h, the PS algorithm can be expressed by the following scheme:

$$[m_1 p_1, m_2 p_2, ..., m_N p_N]. \tag{4}$$

For example, the scheme $[1p_1, 2p_2]$ means that, while the underlying IVP (1) is integrated, the value of p is governed by the sequence of $(p_1, p_2, p_2, p_1, p_2, p_2, p_1, ...)$ with a period of $3h$ and the time-averaged value $p^* = (p_1 + 2 \times p_2)/3$.

2.2. *Numerical Simulation of PS*

To implement numerically the PS algorithm, we consider the Chen chaotic system of non-commensurate fractional order which is evolved from its integer-order counterpart described in [Zhong & Tang, 2002], modeled by the following state equations of fractional-order:

$$\begin{aligned} D_*^{0.92} x_1 &= p(x_2 - x_1), \\ D_*^{0.95} x_2 &= -2.86x_1 + 3.65x_2 - x_1 x_3, \\ D_*^{0.90} x_3 &= x_1 x_2 - 0.30x_3. \end{aligned} \tag{5}$$

Expressed in the form of (1), we have

$$f(x) = \begin{pmatrix} 0 \\ -2.86x_1 + 3.65x_2 - x_1 x_3 \\ x_1 x_2 - 0.30x_3 \end{pmatrix},$$

and

$$A = \begin{pmatrix} -1 & 1 & 0 \\ 0 & 0 & 0 \\ 0 & 0 & 0 \end{pmatrix}.$$

[1]Recently, numerical simulation confirms that PS scheme is also workable for some fractional order systems and similar results are observed [Danca *et al.*, 2012].

Notation 2. SC represents the stable cycle of the fractional-order Chen system (5).

1. Suppose that we want to approximate the SC corresponding to $p = 4.26$, which belongs to a periodic window in the parameter space (see the bifurcation diagram generated for $p \in [4.14, 4.35]$ in Fig. 1). For this purpose we can apply the scheme $[1p_1, 1p_2]$ with $\mathcal{P}_2 = \{4.22, 4.3\}$. The obtained switched SC is plotted (in red) in Fig. 2 (a). From (3), we have $p^* = (4.22 + 4.3)/2 = 4.26$ and the obtained averaged SC is overplotted (in blue) over the switched SC in Fig. 2 (a). A perfect matching between these attractors can be observed with the use of phase plot, and the overplotted time series (Fig. 2 (d)–(f)).
Since the underlying attractors (corresponding to p_1 and p_2) are chaotic (see Fig. 2 (b) and (c)) and the obtained (switched) attractor is a SC, the PS algorithm performs the following paradoxical chaos control-like: $chaos_1 + chaos_2 = order$, where $chaos_{1,2}$ correspond to the chaotic behaviors and *order* characterizes the obtained SC under the PS scheme.
2. If one considers the PS algorithm with $N = 6$ switching values $\mathcal{P}_6 = \{4.19, 4.22, 4.23, 4.29, 4.34, 4.35\}$ and the weights $m_1 = 1$, $m_2 = 2$, $m_3 = 2$, $m_4 = 1$, $m_5 = 3$ and $m_6 = 1$, the corresponding scheme (4): $[1p_1, 2p_2, 2p_3, 1p_4, 3p_5, 1p_6]$, generates the switched attractor which approximates the averaged SC corresponding to $p^* = 4.275$. The match is revealed by the overplots of the switched and averaged SC in the phase space (Fig. 3).
As can be seen in the bifurcation diagram, all the attractors corresponding to p_i, for $i = 1, 2, ..., 6$, are chaotic and a SC is attained by the PS scheme. Therefore one can say that the PS algorithm leads to following chaos control-like: $chaos_1 + chaos_2 + ... + chaos_6 = order$.

Remark 2.1. The necessary condition to achieve a control-like action via the PS algorithm is that p^* must be located inside a periodic window, framed by two chaotic windows.

3. Circuitry Implementation

In order to experimentally implement the PS algorithm, we focus on a circuitry realization of the fractional-order Chen system (5). A switching circuit is to be designed to realize the PS algorithm so that a direct relationship is established.

3.1. *Chen Circuit of Fractional Order*

From the view point of circuitry realization, the distinct difference between an integer-order system and the corresponding fractional-order system lies in the use of fractional integration. For analogue circuit design, the op-amp circuit in Fig 4 (a) is commonly adopted for time integration, presenting a transfer function of $\frac{1}{RCs}$. To convert it into fractional-order integration, the capacitor C in Fig 4 (a) can be replaced by a "fractional capacitor", converting the transfer function to $\frac{1}{RCs^q}$ with $0 < q < 1$. By matching the fractional power frequency response, it can be approximated by a recurrent structure of pole-zero pairs [Ahmad & Sprott, 2003; Charef *et al.*, 1992]:

$$\frac{1}{s^q} \approx \frac{1}{(1 + \frac{s}{p_T})^q} \approx \frac{\prod_{i=0}^{K-1} \left(1 + \frac{s}{z_i}\right)}{\prod_{i=0}^{K-1} \left(1 + \frac{s}{p_i}\right)} \tag{6}$$

where p_T is the corner frequency. The poles and the zeros are with the following recurrence relation:

$$\begin{cases} z_{i-1} = p_{i-1} 10^{\frac{m}{10(1-q)}}, \\ p_i \quad = z_{i-1} 10^{\frac{m}{10q}}, \end{cases}$$

where $i = 1, 2, \cdots, K$ and $p_0 = p_T 10^{\frac{m}{20q}}$. The variable m (in dB) specifies the maximum discrepancy of the frequency responses between the approximation model and the actual system, while the number of pole-zero pairs, K, can be determined by

$$K = 1 + \left\lfloor \frac{log\left(\frac{\omega_{max}}{p_0}\right)}{log(ab)} \right\rfloor, \tag{7}$$

where $a = 10^{\frac{m}{10(1-q)}}$, $b = 10^{\frac{m}{10q}}$ and ω_{max} is the bandwidth of the system.

For example, let $q = 0.92$, $p_T = 0.01$, $\omega_{max} = 100$ and $m = 2$, we have

$$\begin{aligned}\frac{1}{s^{0.92}} &\approx \frac{2.4181(s+4.0616)(s+2118.79)}{(s+0.01284)(s+6.7002)(s+3495.25)} \\ &= \frac{0.8875}{s+0.01284} + \frac{0.5776}{s+6.002} + \frac{0.9530}{s+3495.25},\end{aligned} \tag{8}$$

and the integration circuit in Fig. 4 (a) is transformed to Fig. 4 (b).

Therefore, the realization of the non-commensurate system (5) can be achieved and its circuitry design is given in Fig. 5 while Fig. 6 depicts the corresponding circuits for the approximation of fractional capacitors C_1, C_2 and C_3. In our experiment, it is also assumed that R_3 is the control parameter and r refers to its resistance value.

From Fig. 5, the following state equations can be derived:

$$\begin{aligned}D^{q_1}x &= \frac{1}{R_3C_0}\left(y\frac{R_2}{R_1} - x\frac{R_5R_6}{R_1R_4}\right), \\ D^{q_2}y &= \frac{1}{R_{14}C_0}\left(\frac{R_{13}}{R_{12}}\right)\left[-x\frac{R_9}{R_7} + y\frac{R_{11}}{R_{10}+R_{11}}\right. \\ &\qquad \left.\left(1+\frac{R_9}{R_8}+\frac{R_9}{R_7}\right) - \frac{xz}{10}\frac{R_9}{R_8}\right], \\ D^{q_3}z &= \frac{1}{R_{19}C_0}\left[\frac{xy}{10}\frac{R_{16}}{R_{15}} - z\frac{R_{18}}{R_{17}+R_{18}}\left(1+\frac{R_{16}}{R_{15}}\right)\right].\end{aligned} \tag{9}$$

Based on the given resistors' values, we have

$$\begin{aligned}D^{0.92}x_1 &= \frac{1}{RC_0}\alpha(x_2 - x_1), \\ D^{0.95}x_2 &= \frac{1}{RC_0}(-2.86x_1 + 3.65x_2 - x_1x_2), \\ D^{0.90}x_3 &= \frac{1}{RC_0}(x_1x_2 - 0.30x_3),\end{aligned} \tag{10}$$

with

$$C_0 = 0.47\mu F, \quad R = 510\Omega \quad \text{and} \quad \alpha = \frac{510}{r}, \tag{11}$$

which can be considered as the dimensional form of (5) with a time constant of RC_0.

Figures 7 and 8 depict some representative attractors obtained with the fractional-order Chen's circuit, by increasing α (i.e. decreasing r) in comparison with the attractors obtained by numerical simulations. A close agreement is remarked. Based on these experimental and the numerical results, we obtained the following property to connect the simulation and the experiment to facilitate comparisons later.

Property 3. Between α and p, there exists the following linear relation:

$$p = 0.58\alpha + 2.68. \tag{12}$$

The relation (12) is obtained by line fitting as presented in Fig. 9, where each point represents a representative attractor in simulation and experiment, based on p and α, respectively. A small derivation is noticed but it is always acceptable as tolerance in electronic components is inevitable.

Remark 3.1. Taking into account (11) and the linear relation (12), the following one-to-one mapping between r and p, which connects the experiments and simulation results, can be obtained:

$$p = \frac{295.80}{r} + 2.68. \tag{13}$$

3.2. *Design of Switching Circuit*

In order to allow switching of r in the electronic circuit, a switching circuit given in Fig. 10 is proposed to replace the highlighted block in Fig. 5. Each switch SW_i is implemented by an analog switch MAX4690 [Munir & Canny, 2013] which has a very low on-resistance (1.25 Ω in max) and low off-leakage current (0.5nA in max at 25^oC). SW_i, $i = 1, 2, \cdots$ is opened and closed by applying 0V and 5V to $\eta_i(t)$, $i = 1, 2, \cdots$ respectively. However, due to the hard switching of MOSFETs, high frequency oscillations have been induced. To reduce the adverse effect to the system, a small shunt capacitor ($C_s = 10nF$) is added to filter the spikes.

To switch r among N different values, $(N-1)$ switches are needed and the followings are assumed.

Assumption 4.
1. A square signal $\eta_i(t)$ of period T_i is used to switch on/off the resistor $R_{3,i}$, $i = 1, 2, ...(N-1)$. $f_i = 1/T_i$ and D_i stand for the frequency and duty cycle of $\eta_i(t)$, respectively.
2. For all i, $f_i = f$ ($f = 10KHz$ in our experiment) and $D_{i+1} < D_i$.
3. The rising edges of all $\eta_i(t)$ are synchronized.

The elements of the switching set $\mathcal{R}_N = \{r_1, r_2, \cdots, r_N\}$ can be obtained by

$$r_i = \left(\sum_{k=0}^{N-i} \frac{1}{R_{3,k}} \right)^{-1} \tag{14}$$

where $i = 1, 2, \cdots, N$.

For example, for $N = 2$, only a single switching circuit is necessary, and we have $\mathcal{R}_2 = \{r_1, r_2\}$, where $r_1 = \left(R_{3,0}^{-1} + R_{3,1}^{-1} \right)^{-1}$ and $r_2 = R_{3,0}$.

Reversely, $R_{3,i}$ can be obtained by

$$R_{3,i} = \left(\frac{1}{r_{N-i}} - \frac{1}{r_{N-i+1}} \right)^{-1} \tag{15}$$

where $i = 1, 2, \cdots, N-1$ and $R_{3,0} = r_N$.

The weights of r_i in switching, m_i', are given by

$$m_i' = 100 \times (D_{N-i} - D_{N-i+1}) \tag{16}$$

where $i = 1, 2, \cdots, N$, $D_N = 0$ and $D_0 = 1$.

Note: A factor of 100 is included because the duty cycle is expressed in percentage, and $\sum_i^N m_i' = 100$.

Reversely, we can have the following iterative function

$$D_{N-i} = 0.01 \times m_i' + D_{N-i+1} \tag{17}$$

where $i = 1, 2, \cdots, (N-1)$ and $D_N = 0$.

Considering a fixed time interval $h' = 1/(100f) = 1\mu s$, m_i' are the correspondents of the weights m_i in the scheme (4). As a result, together with (13), (14) and (16), the switching circuit in Fig. 10 can be considered as working schematically as following the scheme:

$$[m_1' r_1, m_2' r_2, ...m_N' r_N], \tag{18}$$

which is equivalent to (4).

Given a set $\mathcal{R}_N$, similarly with the time-averaged value p^*, the time-averaged resistance r^* is given by

$$r^* := \frac{\sum_{i=1}^N m_i' r_i}{\sum_{i=1}^N m_i'}. \tag{19}$$

Remark 3.2. The solution to (3) or (19) is not unique (there are infinitely sets of values for p_i (r_i) and m_i (m_i') to obtain the same value p^* (r^*)). Therefore the same attractor can be obtained with several switching schemes (4) or (18).

4. Experimental Verification of "Chaos+Chaos=Order"

The circuit in Sec. 3 is used and the PS algorithm is experimentally applied. To approximate the SC corresponding to some value of r, we have to firstly find a suitable set of $\mathcal{R}_N$ and m_i', $i = 1, 2, ..., N$, such that the time-averaged value (using (19)) is equal to the targeted value. Then, with the Assumption 4, the corresponding values of $R_{3,i}$, $i = 0, 1, \cdots, (N-1)$ and D_j, $j = 1, 2, \cdots, (N-1)$ can be found by (15) and (17).

In the followings, the cases of $N = 2$ and $N = 3$ are considered and SCs situated in the largest periodic window framed by the chaotic windows are to be approximated (see Remark 2.1 and Fig. 1).

4.1. *Experimental Results*

1. Suppose we want to obtain the SC corresponding to $r = 188\Omega$ and the scheme $[50r_1, 50r_2]$ is used. In this case, $N = 2$ and only a single switch (SW1) is needed. Let $\mathcal{R}_2 = \{181, 195\}$, from (19) we have $\frac{1}{100}(50 \times 181 + 50 \times 195) = 188$ and hence the time-averaged r^* is equal to our target value. Based on (15), we derive that

$$R_{3,0} = 195\Omega$$
$$R_{3,1} = (1/181 - 1/195)^{-1} = 2521\Omega$$

and

$$D_1 = 0.01 \times 50 + 0 = 0.5.$$

Based on the switching circuit in Fig. 10, we complete our design by using a square signal $\eta_1(t)$ of frequency 10KHz and duty cycle of 50%, together with resistors $R_{3,0} = 195\Omega$ and $R_{3,1} = 2521\Omega$. The switched SC is obtained as shown in Fig. 11 (c). For comparison, we obtained the sampled data of the "switched" attractor and the "averaged" attractor based on a fixed value $r = r^* = 188\Omega$. As shown by the overplot in Fig. 11 (d), these two attractors match very well.
It should be pointed out that, when SW1 is always OPENED, $r = r_1 = 195\Omega$ and a chaotic attractor is obtained as depicted in Fig. 11 (a). Similarly, when SW1 is CLOSED, $r = r_2 = 181\Omega$ and the attractor is also chaotic (see Fig. 11 (b)). Since the attractors corresponding to r_1 and r_2 are chaotic and the "switched" SC is a regular stable motion (*order*), the PS algorithm leads to the following paradoxical chaos control-like: $chaos_1 + chaos_2 = order$.
2. As stated in Remark 3.2, we can obtain the same SC with different switching schemes. Let's consider another scheme $[60r_1, 40r_2]$ with $\mathcal{R}_2 = \{183.33, 195\}$, such that $\frac{1}{100}(60 \times 183.33 + 40 \times 195) = 188$. Based on (15) and (17), we can obtain $R_{3,0} = 195\Omega$, $R_{3,1} = 3064\Omega$ and the duty cycle of $\eta_1(t)$ is $D_1 = 60\%$. The obtained "switched" attractor is shown in Fig. 12 (c). Again, a close match is observed from the overplot of the "switched" attractor and the "averaged" attractor given in Fig. 11 (d). Similar to the previous case, we have $chaos_1 + chaos_2 = order$, where $chaos_{1,2}$ correspond to the chaotic attractors for $r_{1,2}$ (see Fig. 12 (a) and (b)).
3. Finally, let's consider the case of $N = 3$. Two analog switches are then needed, and the PS scheme $[40r_1, 20r_2, 40r_3]$ with $\mathcal{R}_3 = \{172.5, 195, 200\}$ is employed. Following (18), $0.4 \times 172.5 + 0.2 \times 195 + 0.4 \times 200 = 188$ which is our targeted value. From (15) and (17), we obtain

$$R_{3,0} = 200\Omega$$
$$R_{3,1} = (1/195 - 1/200)^{-1} = 7800\Omega$$
$$R_{3,2} = (1/172.5 - 1/195)^{-1} = 1495\Omega$$

and

$$D_2 = 0.01 \times 40 = 40\%$$
$$D_1 = 0.01 \times 20 + 0.4 = 60\%.$$

The "switched" SC is depicted in Fig. 13 (d). It can be observed that, although it is much more noisy than the previous two cases, the SC is still retained. A close match between the "switched" SC attractor and

the "averaged" SC attractor is revealed by the overplot in Fig. 13 (e). Because the underlying attractors corresponding to $r_{1,2,3}$ are chaotic (Fig. 13 (a), (b) and (c)), the following control-like scheme is obtained: $chaos_1 + chaos_2 + chaos_3 = order$.

4.2. *Discussions*

Both the simulation and experimental results show that the attractors obtained by switching the parameter and using a fixed time-averaged parameter could be the same. This is true when the switching frequency f is high enough in simulation (i.e. h is small). Similar case is found in experiment and f is to be high too. However, f cannot be too high due to the bandwidth of the switching component in use. In addition, there is difference between the switch-on and switch-off time for the analog switch ($t_{on} = 130ns$ and $t_{off} = 90ns$ typical for MAX4690), which induce inaccuracy in D_i. When f is higher, this error becomes more significant.

Another problem that occurs in experiment is due to the noise caused by the hard switching of the analog switch. As mentioned in Sec. 3, that can be resolved by adding a small shunted capacitor. A significant reduction of noise is noticed but it will also reduce the bandwidth. Figure 14 shows the case when the shunted capacitor is removed. It is remarked that the high level of noise may make the obtained attractor being unstable (Note: Fig. 14 is a snapshot of the attractor and sometimes the trajectory may escape from the attractor and return.)

There are several potential applications for the PS algorithm. Firstly, it provides a means to generate different attractors by simply switching a parameter. In case that certain value cannot be assigned in practice, this procedure gives a flexible way to obtain the desired attractor. Secondly, as demonstrated in our numerical and experimental results, it is possible to achieve chaos control by switching a system parameter, and the dynamics of a system can be changed from chaotic to periodic. Also, since the property (1) is general, chaotic attractor can also be obtained by PS, and hence anticontrol is also possible (see e.g. [Danca *et al.*, 2008]).

5. Conclusions

It is the first to realize the PS scheme and to demonstrate its effectiveness in practice. Our work focuses on the fractional-order Chen system, which can be modeled by a set of FDEs and realized in an electronic circuit. By comparing the experimental and simulation results obtained from the circuit and numerical solver, respectively, a close match is found even they adopted different approaches of approximation. It is concluded from both the simulation and experiments that an attractor obtained under PS is close to the attractor with a fixed parameter set as the time-averaged of the switched values. Lastly, some practical issues in related to the implementation of PS scheme, such as the switching time and the switching noise, have been discussed. Although limitations in circuitry realization of PS scheme are inevitable, our work can still well confirm the practicability of the scheme.

References

Agrawal, S.K., Srivastava, M. & Das, S. [2012] "Synchronization of fractional order chaotic systems using active control method," *Chaos Soliton Fract.* **45(6)**, 737–752.

Ahmad, W.M. & Sprott, J.C. [2003] "Chaos in fractional-order autonomous nonlinear systems," *Chaos Soliton Fract.* **16(2)**, 339–351.

Asheghan, M.M., Beheshti, M.T.H. & Tavazoei, M.S. [2011] "Robust synchronization of perturbed Chen's fractional-order chaotic systems," *Commun. Nonlinear Sci.* **16(2)**, 1044–1051.

Caputo, M. [1967] "Linear models of dissipation whose Q is almost frequency independent–II," *Geophys. J. R. Astron. Soc.* **13(5)** 529–539.

Charef, A., Sun, H.H., Tsao, Y.Y. & Onaral, B. [1992] "Fractal system as represented by singularity function," *IEEE T. Automat. Contr.* **37(9)**, 1465–1470.

Danca, M.F., Tang, W.K.S. & Chen, G. [2008] "A switching scheme for synthesizing attractors of dissipative chaotic systems," *Appl. Math. Comput.* **201(1-2)**, 650–667.

Danca, M.F., Romera, M., Pastor, G. & Montoya, F. [2012] "Finding attractors of continuous-time systems by parameter switching," *Nonlinear Dynam.* **67(4)**, 2317–2342.

Danca, M.F., Bourke, P. & Romera, M. [2013] "Graphical exploration of the connectivity sets of alternated Julia sets; M, the set of disconnected alternated Julia sets," *Nonlinear Dynam.* **73**, 1155–1163.

Danca, M.F., Fečkan, M. & Romera, M. [2014] "Generalized form of Parrondo' s paradoxical game with applications to chaos control," *Internat. J. Bifur. Chaos* **24(1)**, 1450008.

Diethelm, K., Ford, N.J. & Freed, A.D. [2002] "A predictor-corrector approach for the numerical solution of fractional differential equations," *Nonlinear Dynam.* **29(1)**, 3–22.

Dzieliński, A., Sierociuk, D. & Sarwas, G. [2010] "Some applications of fractional order calculus," *B Pol. Acad. Sci-Tech* **58(4)**, 583–592.

Foias, C. & Jolly, M.S. [1995] "On the numerical algebraic approximation of global attractors," *Nonlinearity* **8(3)**, 295–319.

Galvao, R.K.H., Hadjiloucas, S., Kienitz, K.H. & Paiva, H.M. [2013] "Fractional order modeling of large three-dimensional RC networks," *IEEE T. Circuits-I* **60(3)**, 624–637.

Gammoudi, I.E. & Feki, M. [2013] "Synchronization of integer order and fractional order Chua's systems using robust observer," *Commun. Nonlinear Sci.* **18(3)**, 625–638.

Hegazi, A.S., Ahmed, E. & Matouk, A.E. [2013] "On chaos control and synchronization of the commensurate fractional order Liu system," *Commun. Nonlinear Sci.* **18(5)**, 1193–1202.

Jia, H.Y., Chen, Z.Q. & Qi, G.Y. [2014] "Chaotic characteristics analysis and circuit implementation for a fractional-order system," *IEEE T. Circuits-I* **61(3)**, 845–853.

Kaslik, E. & Sivasundaram, S. [2012] "Non-existence of periodic solutions in fractional-order dynamical systems and a remarkable difference between integer and fractional-order derivatives of periodic functions," *Nonlinear Anal-Real.* **13(3)**, 1489–1497.

Kingni, S.T., Nana, B., Mbouna Ngueuteu, G.S., Woafo, P. & Danckaert, J. [2015] "Bursting oscillations in a 3D system with asymmetrically distributed equilibria: Mechanism, electronic implementation and fractional derivation effect," *Chaos Soliton Fract.* **71**, 29–40.

Lin, T.C., Lee, T.Y. & Balas, V.E. [2011] "Adaptive fuzzy sliding mode control for synchronization of uncertain fractional order chaotic systems," *Chaos Soliton Fract.* **44(10)**, 791–801.

Liu, L., Liu, C. & Zhang, Y. [2009] "Experimental verification of a four-dimensional Chua's system and its fractional order chaotic attractors," *Internat. J. Bifur. Chaos* **19(8)**, 2473–2486.

Mao. Y., Tang, W.K.S. & Danca, M.F. [2010] "An averaging model for chaotic system with periodic time-varying parameter," *Appl. Math. Comput.* **217(1)**, 355–362.

Munir, Y. & Canny, D. [2013] "Selecting the right CMOS analog switch," *Maxim. Appl. Note.* 5299.

Oldham, K.B. & Spanier, J. [1974] *The Fractional Calculus: Theory and Applications of Differentiation and Integration of Arbitrary Order,* (Academic Press, New York).

Parreño, A., Roncero-Sánchez, P., del Toro García, X., Feliu, V. & Castllo, F. [2010] "Analysis of the fractional dynamics of an ultracapacitor and its application to a buck-boost converter," In: Baleanu, D., Güvenc, Z.B. & Tenreiro Machado J.A., editors. New Trends in Nanotechnology and Fractional Calculus Applications, Springer Science+Business Media B.V., 97–105.

Podlubny, I. [2002] "Geometric and physical interpretation of fractional integration and fractional differentiation," *Fract. Calc. Appl. Anal.* **5(4)**, 367–386.

Shen, Y., Yang, S. & Sui, C. [2014] "Analysis on limit cycle of fractional-order van der Pol oscillator," *Chaos Soliton Fract.* **67**, 94–102.

Sun, K., Wang, X. & Sprott, J.C. [2010] "Bifurcation and chaos in fractional-order simplified Lorenz system," *Internat. J. Bifur. Chaos* **20(4)**, 1209–1219.

Tavazoei, M.S. & Haeri, M. [2010] "Rational approximations in the simulation and implementation of fractional-order dynamics: A descriptor system approach," *Automatica* **46(1)**, 94–100.

Wang, X., He, Y. & Wang, M. [2009] "Chaos control of a fractional order modified coupled dynamos system," *Nonlinear Anal.-Theor.* **71(12)**, 6126–6134.

Xu, F. [2014] "The generation of a series of multiwing chaotic attractors using integer and fractional order differential equation systems," *Internat. J. Bifur. Chaos* **24(10)**, 1450130.

Yazdani, M. & Salarieh, H. [2011] "On the existence of periodic solutions in time-invariant fractional order

systems," *Automatica* **47(8)**, 1834–1837.
Zhang, C. & Yu, S. [2011] "Generation of multi-wing chaotic attractor in fractional order system," *Chaos Soliton Fract.* **44(10)**, 845–850.
Zhong, G.Q. & Tang, W.K.T. [2002] "Circuitry implementation and synchronization of Chen's attractor," *Internat. J. Bifur. Chaos* **12(6)**, 1423–1427.

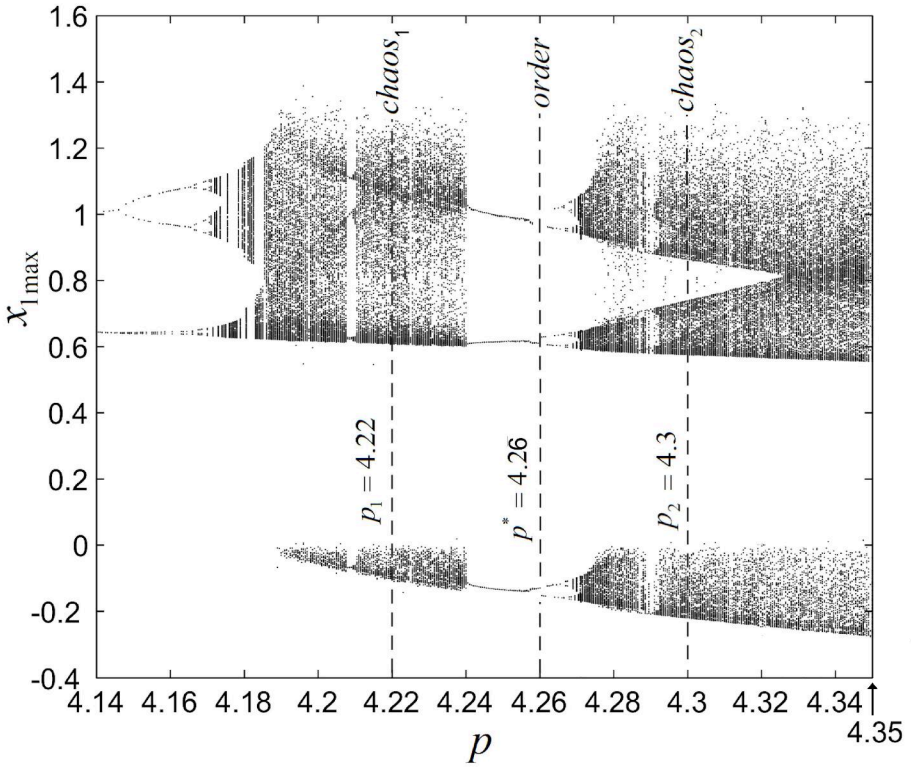

Fig. 1. Bifurcation diagram of the fractional-order Chen system (5) for $p \in [4.14, 4.35]$.

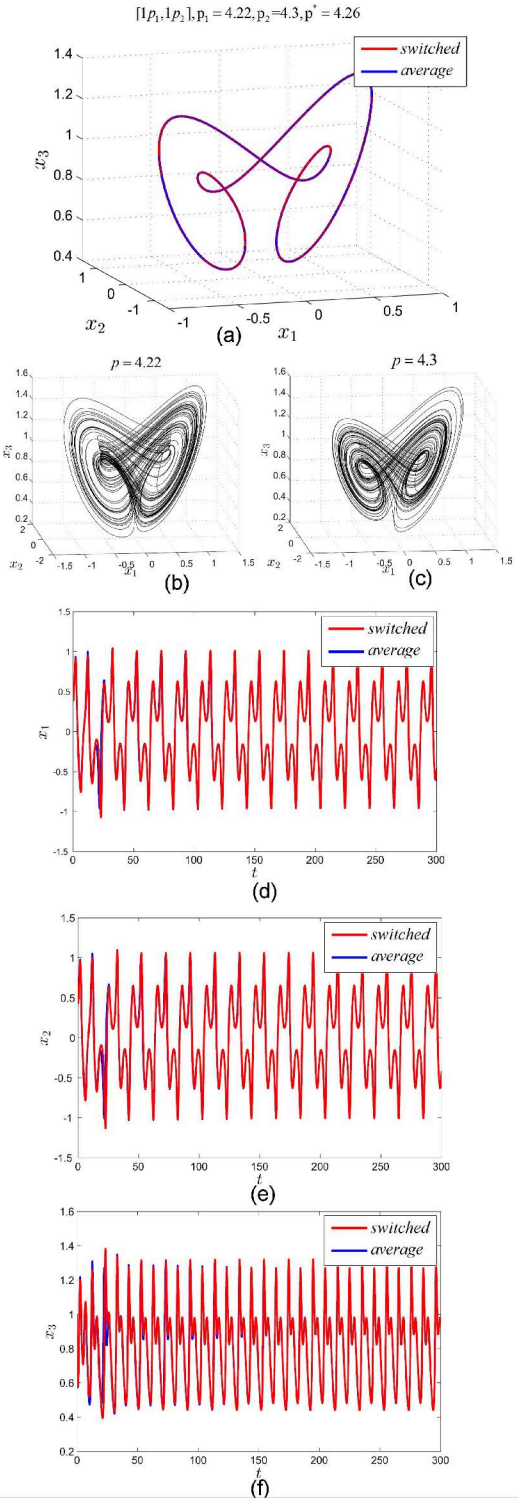

Fig. 2. Switching simulation results with $N = 2$ under the scheme $[1p_1, 1p_2]$ and $\mathcal{P}_2 = \{4.22, 4.3\}$ (a) Overplots of the averaged SC (blue) corresponding to $p^* = 4.26$ and switched SC (red) (b) Chaotic attractor corresponding to $p = 4.22$; (c) Chaotic attractor corresponding to $p = 4.3$; (d)-(f) Overplotted time series of the two SCs.

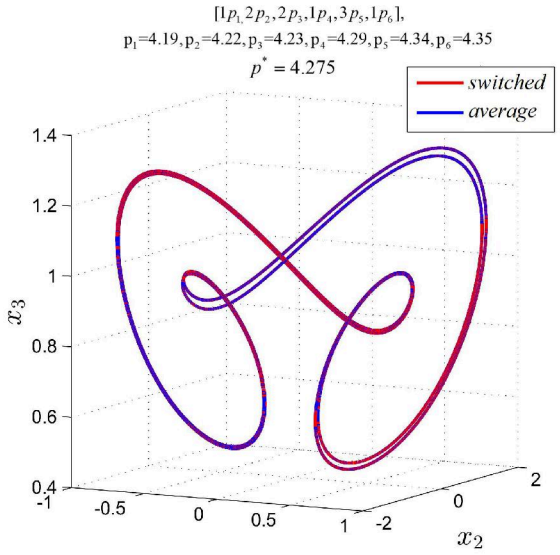

Fig. 3. Switching simulation results with $N = 6$, under the scheme $[1p_1, 2p_2, 2p_3, 1p_4, 3p_5, 1p_6]$ and $\mathcal{P}_6 = \{4.19, 4.22, 4.23, 4.29, 4.34, 4.35\}$; $p^* = 4.275$.

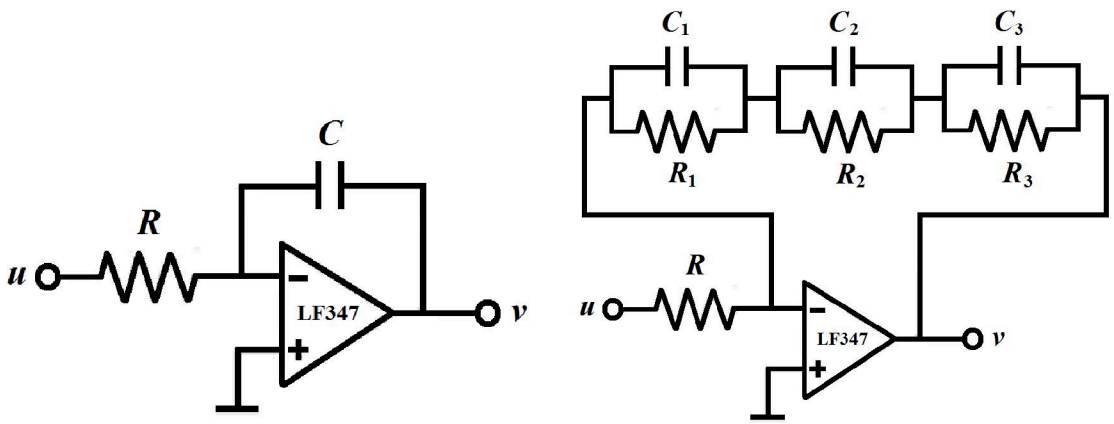

(a) (b)

Fig. 4. Integration with opamp circuit (a) $C = 0.47\mu F$ (b) $C_1 = 530nF$, $C_2 = 814nF$, $C_3 = 493nF$, $R_1 = 146.95M\Omega$, $R_2 = 183.35K\Omega$, $R_3 = 580\Omega$.

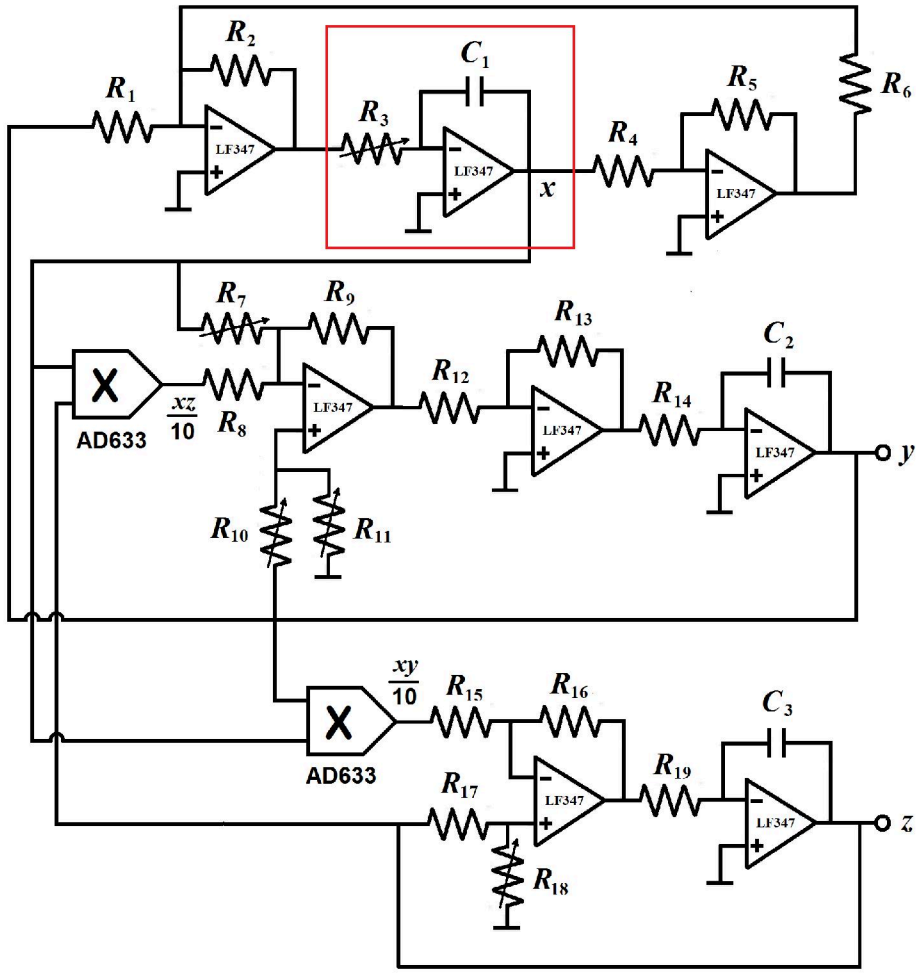

Fig. 5. Realization of Fractional-order Chen system (5). $R_1, R_2, R_4, R_5, R_6, R_9, R_{12}, R_{13}, R_{16}, R_{17} : 10K\Omega$; $R_3 : r\Omega$; $R_7 : 3.492K\Omega$; $R_8, R_{15} : 1K\Omega$; ; $R_{10} : 181\Omega$; $R_{11} : 64.6\Omega$; $R_{14}, R_{19} : 510\Omega$; $R_{18} : 281.2\Omega$.

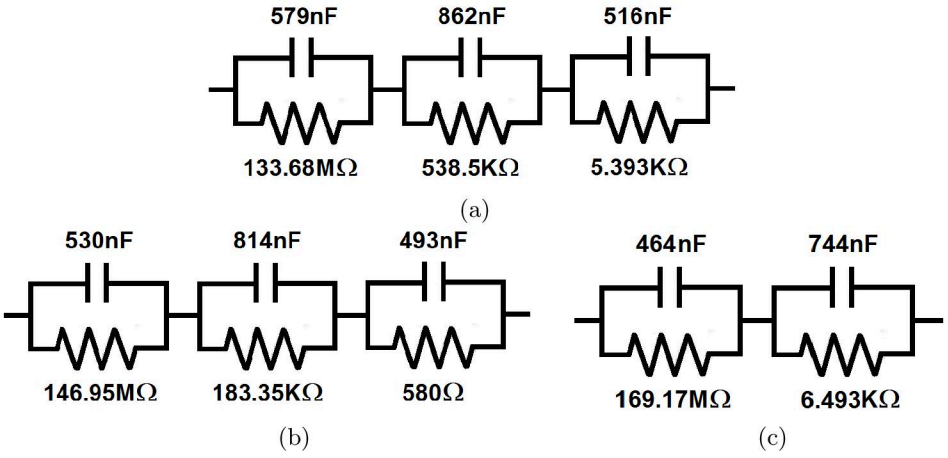

Fig. 6. Approximation of fractional capacitor with (a) $q = 0.95$ (b) $q = 0.92$ (c) $q = 0.90$.

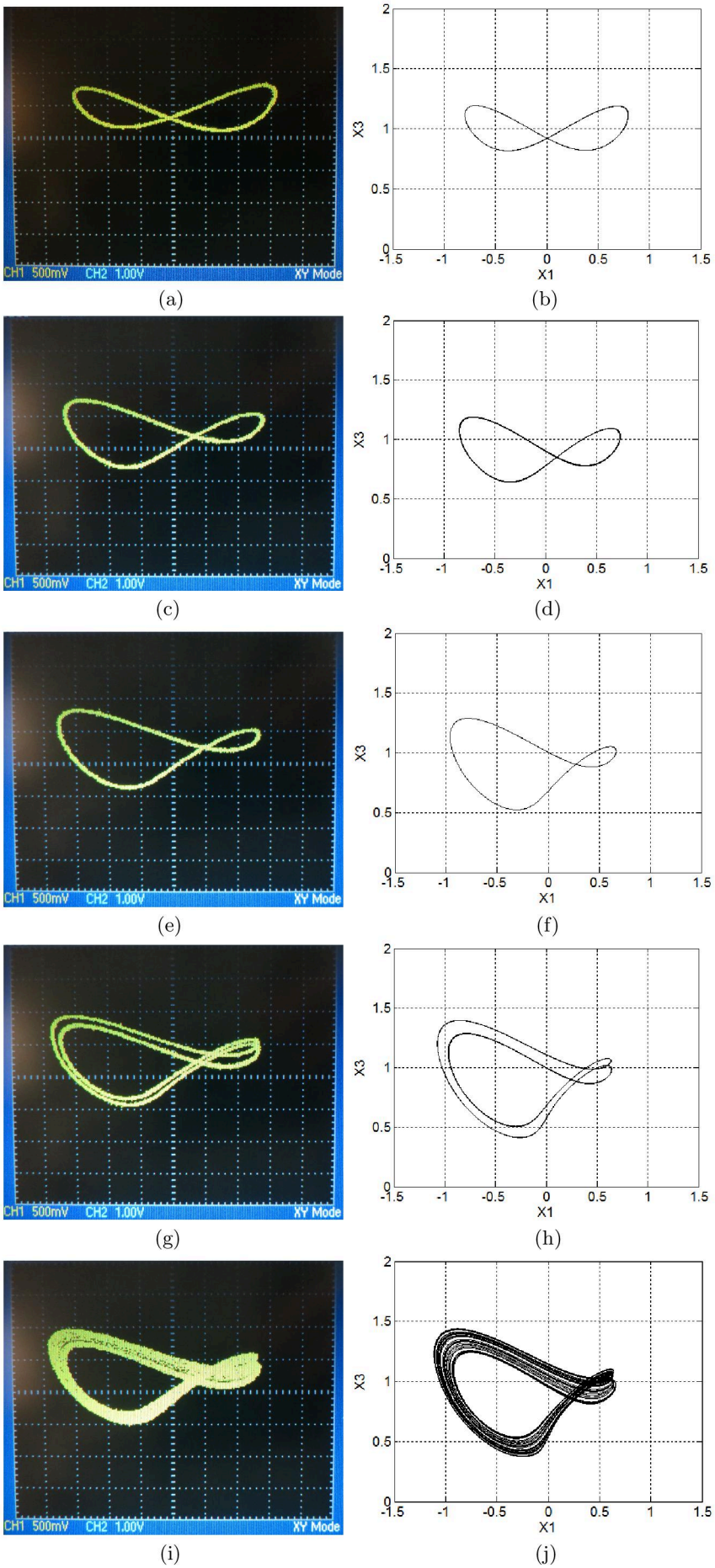

Fig. 7. Attractors obtained in experiment (left-hand column) and simulations (right-hand column) with (a) $r = 243.5(\alpha = 2.094)$; (b) $p = 3.8$; (c) $r = 213.4(\alpha = 2.390)$; (d) $p = 4.03$; (e) $r = 208.4(\alpha = 2.447)$; (f) $p = 4.1$; (g) $r = 208(\alpha = 2.452)$; (h) $p = 4.16$; (i) $r = 205.5(\alpha = 2.482)$; (j) $p = 4.173$.

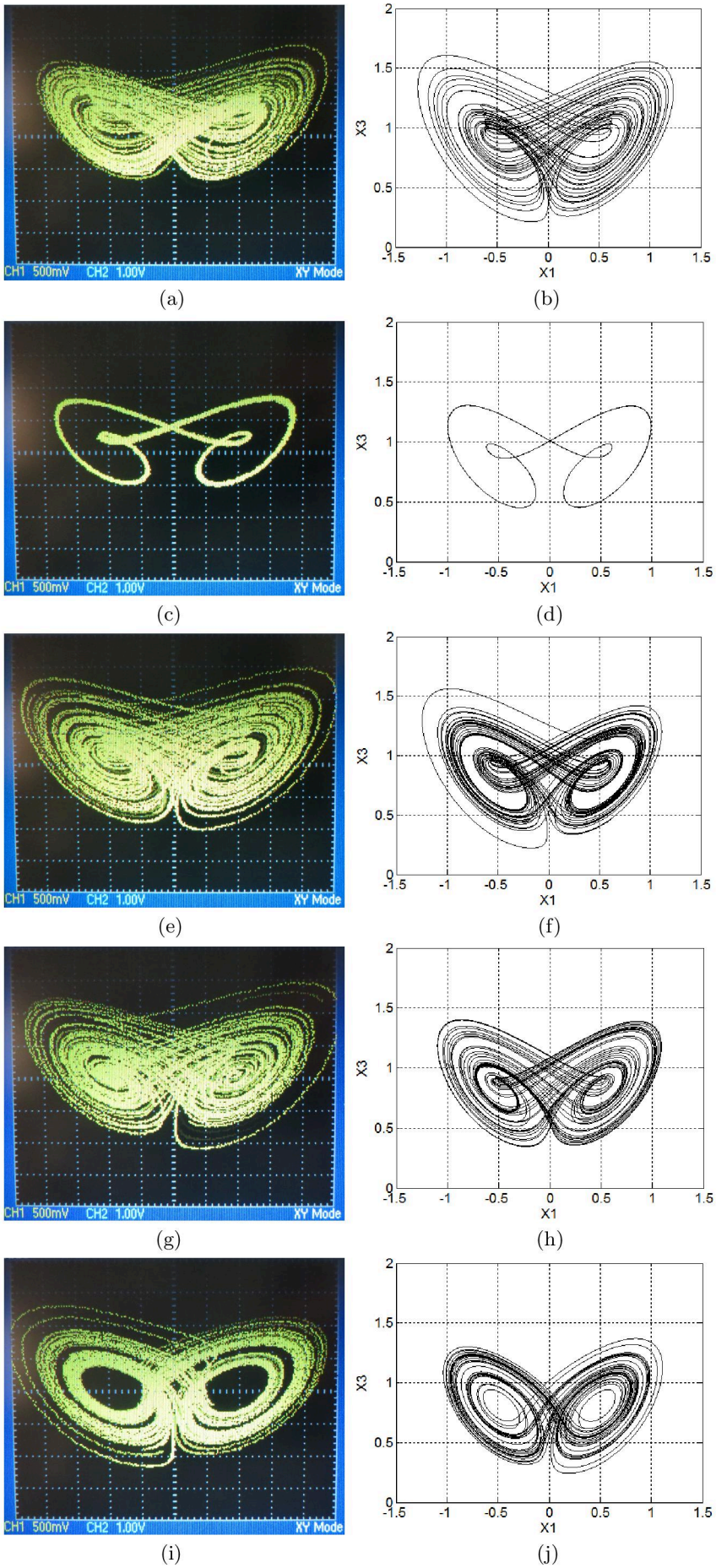

Fig. 8. Attractors obtained in experiment (left-hand column) and simulations (right-hand column) with (a) $r = 204.5(\alpha = 2.494)$; (b) $p = 4.21$; (c) $r = 188(\alpha = 2.713)$; (d) $p = 4.25$; (e) $r = 185.5(\alpha = 2.749)$; (f) $p = 4.3$; (g) $r = 167.8(\alpha = 3.039)$; (h) $p = 4.4$; (i) $r = 130(\alpha = 3.923)$; (j) $p = 4.95$.

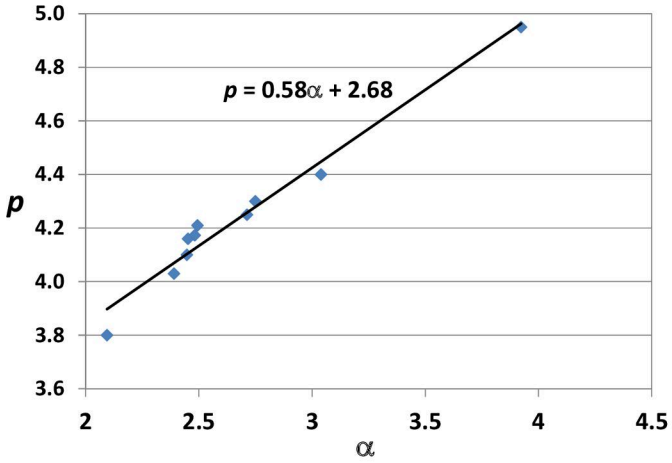

Fig. 9. Relationship between p in (5) and α in (10).

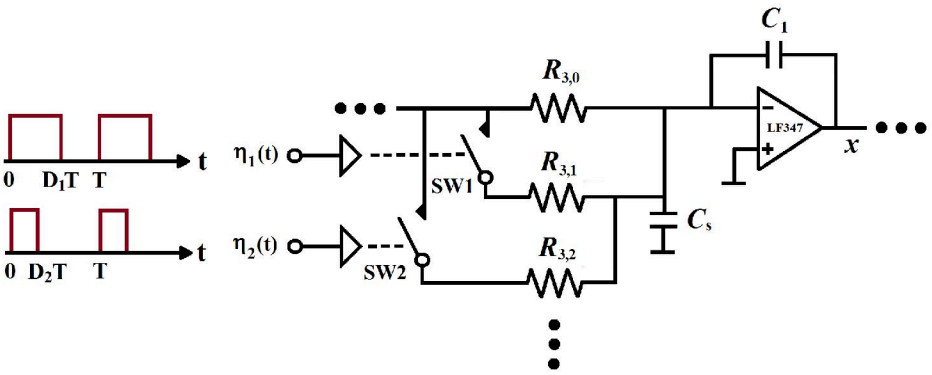

Fig. 10. Switching circuit to switch R_3 between different r. By controlling the on-off states of SW1 and SW2 using $\eta_1(t)$ and $\eta_2(t)$, we can have $r_1 = R_{3,0}//R_{3,1}//R_{3,2}$, $r_2 = R_{3,0}//R_{3,1}$, $r_3 = R_{3,0}$ when $t \in [nT, (n+D_2)T)$, $t \in [(n+D_2)T, (n+D_1)T)$, $t \in [(n+D_1)T, (n+1)T)$, respectively, for $n = 0, 1, 2, \cdots$, and hence $m_1' : m_2' : m_3' = D_2 : (D_1 - D_2) : (1 - D_1)$.

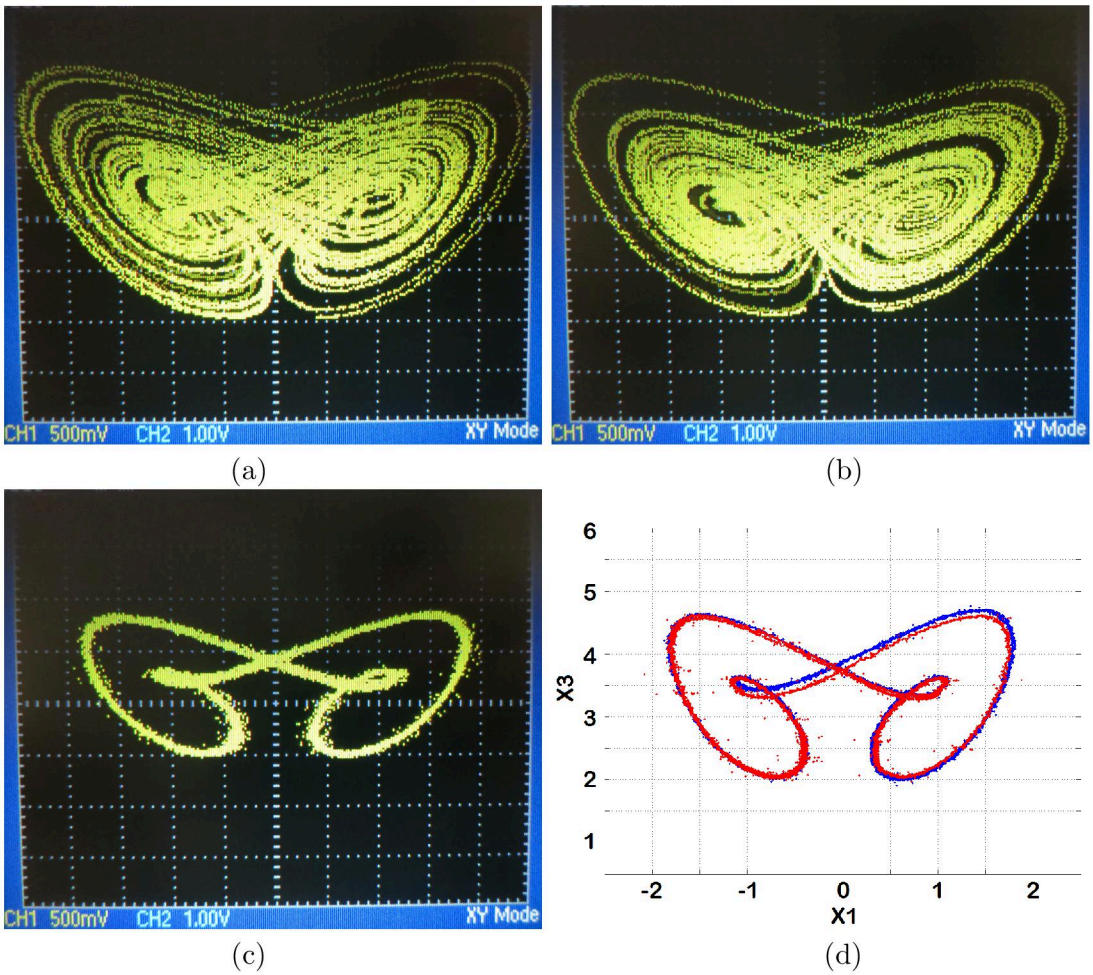

Fig. 11. Experimental switching results with one switch (SW1) and two resistors ($R_{3,0} = 195\Omega$, $R_{3,1} = 2521\Omega$): (a) Chaotic attractor with SW1 always OPENED ($r = r_1 = 195\Omega$) (b) Chaotic attractor with SW1 always CLOSED ($r = r_2 = 181\Omega$) (c) Resultant attractor obtained with the switching scheme $[50r_1, 50r_2]$ (d) Comparison of the averaged SC (blue) corresponding to $r = r^* = 188\Omega$, and the switched SC (red).

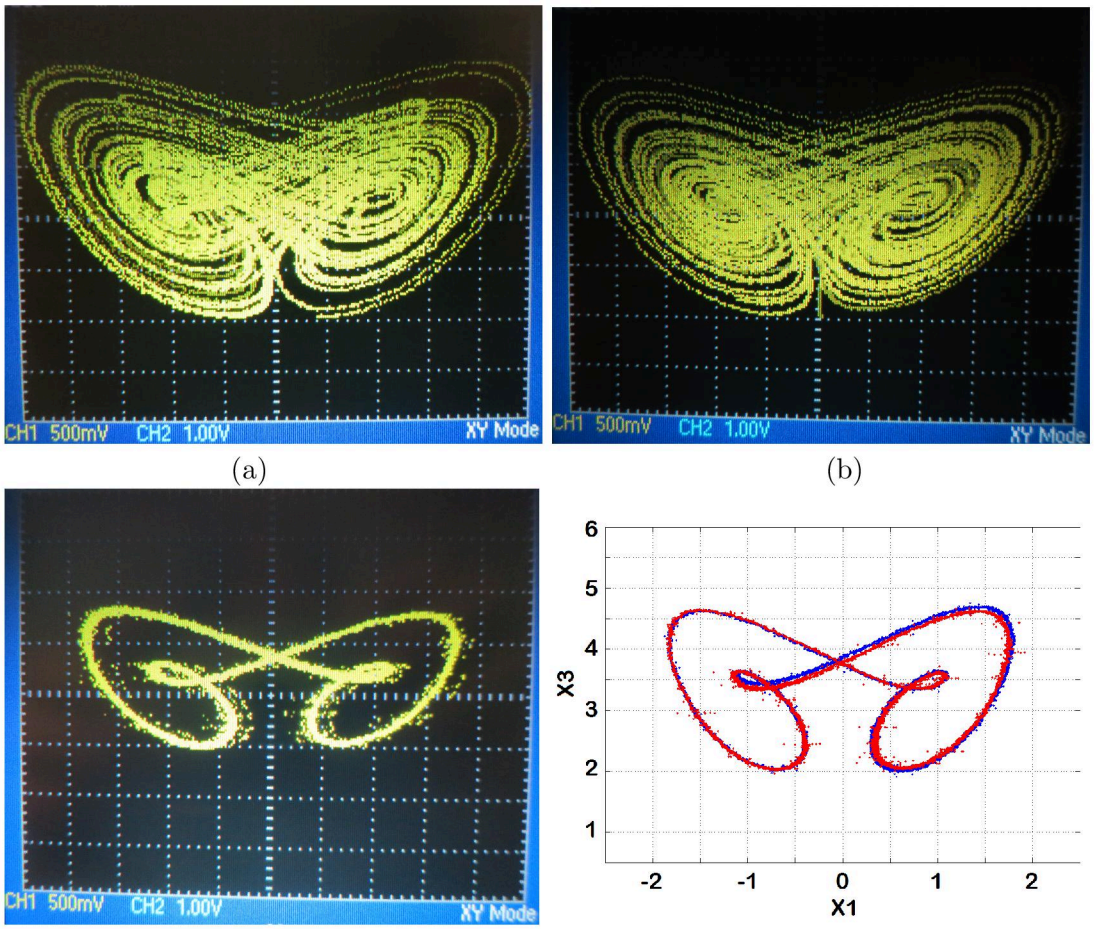

Fig. 12. Experimental switching results with one switch (SW1) and two resistors ($R_{3,0} = 195\Omega$, $R_{3,1} = 3064\Omega$):(a) Chaotic attractor with SW1 always OPENED ($r = r_1 = 195\Omega$); (b) Chaotic attractor with SW1 always CLOSED ($r = r_2 = 183.33\Omega$) (c) Resultant attractor obtained with the switching scheme $[60r_1, 40r_2]$ and $\mathcal{R}_2 = \{183.33, 195\}$ (d) Comparison of the averaged SC (blue) corresponding to $r = r^* = 188$, and the switched SC (red).

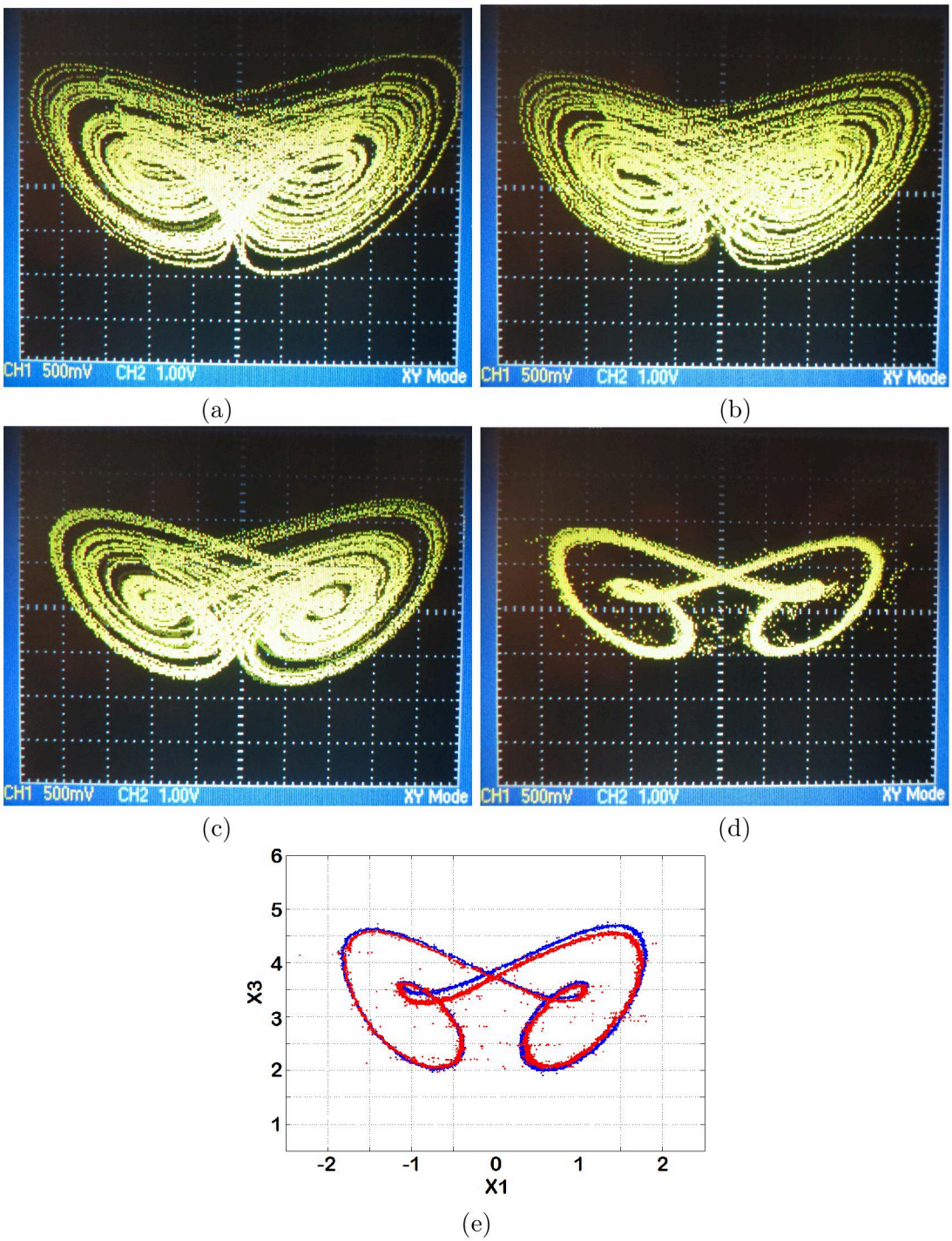

Fig. 13. Experimental switching results with two switches (SW1, SW2) and three resistors ($R_{3,0} = 200\Omega$, $R_{3,1} = 7800\Omega$, $R_{3,2} = 1495\Omega$): (a) Chaotic attractor with SW1 and SW2 always OPENED ($r = r_1 = 200\Omega$) (b) Chaotic attractor with SW1 always CLOSED and SW2 always OPENED ($r = r_2 = 195\Omega$) (c) Chaotic attractor with SW1 and SW2 always CLOSED ($r = r_3 = 172.5\Omega$) (d) Resultant SC with the switching scheme $[40r_1, 20r_2, 40r_3]$ and $\mathcal{R}_3 = \{172.5, 195, 200\}$ (e) Comparison of the averaged SC (blue) corresponding to $r^* = 188$, and the switched SC (red).

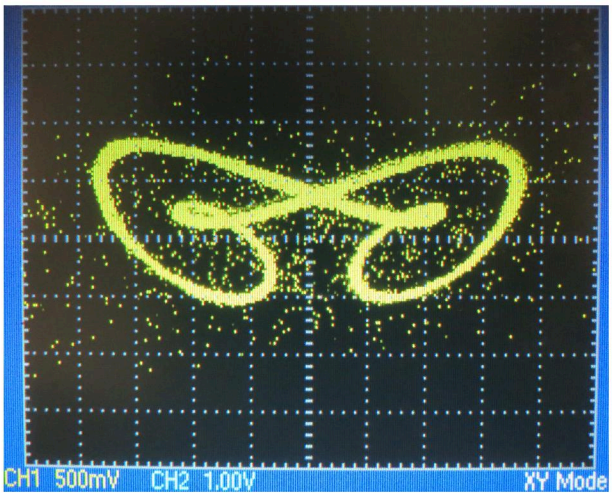

Fig. 14. Experimental result of Case 1 with shunted capacitor being removed.